



# Influence of welding stresses on relief cracking during heat treatment of a creep-resistant 13CrMoV steel: part I—effect of heat control on welding stresses and stress relief cracking

A. Kromm<sup>1</sup> · T. Lausch<sup>1</sup> · D. Schroepfer<sup>1</sup> · M. Rhode<sup>1,2</sup> · T. Kannengiesser<sup>1,2</sup>

Received: 27 December 2019 / Accepted: 27 February 2020  
© The Author(s) 2020, corrected publication 2021

## Abstract

The avoidance of failures during the fabrication or operation of petrochemical reactors made of creep-resistant, low-alloy steels as 13CrMoV9-10 requires still research despite over 60 years of international investigations in the field of stress relief cracking. The quality of modern base materials and filler metals leads to the fact that previously known crack causes, such as impurities of S or P, recede into the background. Rather, the causes are increasingly to be found in the fabrication process. Investigations on the influence of heat control on the stresses in welded components and thus on the stress relief cracking sensitivity under realistic manufacturing conditions are not yet available. This work is subdivided in two parts. Part I of this study focused on the effect of heat control during submerged arc welding on the stresses. For this purpose, a testing facility was applied, which allows to observe the forces and moments accumulating during welding or heat treatment in a component-like specimen under shrinkage restraint. The stress acting in the specimen increases with higher preheat/interpass temperatures and higher heat input. During the heat treatment, the stresses are relieved. Nevertheless, cracks are formed already during heating. The total crack length correlates with the heat input.

**Keywords** Welding · Creep-resistant steel · Post weld heat treatment · Stress relief cracking

## 1 Introduction

In petrochemical reactors, e.g., for hydrocrackers and thick-walled high-temperature hydrogen pressure vessels, low-alloy, bainitic Cr-Mo-(V)-steels are primarily applied. These steels are characterized by their high-temperature strength, good hydrogen pressure resistance, and long service life under creep loads. For process temperatures of up to 482 °C and hydrogen pressures of up to 34.5 MPa, necessary to produce modern synthetic fuels, a modified conventional low-alloyed 2.25Cr-1Mo steel with 0.25% vanadium was developed [1].

Applied largely in petrochemical reactor construction since the mid-1990s, this micro-alloyed steel 13CrMoV9-10 exhibits significantly improved creep resistance at higher temperatures and higher resistance to high-temperature hydrogen attack [2]. However, the V modification of these modern steels results in severe challenges regarding welding processing for the usually very large components. Petrochemical reactors are characterized by wall thicknesses of up to 475 mm, diameters of up to 8 m, a length of up to 30 m, and weights of several 100 t, which leads to a fabrication in numerous individual steps over a period of several months [1]. Additionally, a final heat treatment of the complete vessel (PWHT) is applied after completion of all welding steps in order to adjust the mechanical properties in the weld metal and the heat-affected zone (HAZ) as well as to reduce welding-related structural and residual stresses. Due to the low toughness, high hardness, and high strength of the Cr-Mo-V joints in the as-welded state, an extremely careful handling of the components is needed.

Even though a heat treatment operation will be carried out very diligently, it is of utmost importance to take into account the high sensitivity of this V-modified material towards stress relief cracking (SRC). This kind of cracking can occur during

---

Recommended for publication by Commission II - Arc Welding and Filler Metals

✉ A. Kromm  
ame.kromm@bam.de

<sup>1</sup> Bundesanstalt für Materialforschung und -prüfung (BAM), Berlin, Germany

<sup>2</sup> Institute for Materials Science and Joining Technology, Otto-von-Guericke-University, Magdeburg, Germany

intermediate annealing, PWHT, and during service. The crack formation is also linked to technological phenomena in which initially dissolved precipitates are precipitated again during reheating and lead to differences in strength between the grain interior and the grain boundaries [3, 4]. Hence, the formation of cracks is essentially influenced by the interaction of thermal, metallurgical, and mechanical factors also with regard to welding-related stresses, which can already be critical during production [5]. In general, the crack usually follows an intergranular path along the prior austenite grain boundaries (PAGB) both transversely and longitudinally to the welding direction. Metallurgical and thermal mechanisms of SRC were extensively studied in the last decade, e.g., [6–20]. Therefore, part II of this study gives a review of studies and concepts dealing with the prevention of SRC [21].

It remains to be noted that the procedures for testing materials prone to SRC are usually limited to single-pass welds and the use of small-scale specimens. This generally precludes the use of production-relevant welding technology and realistic manufacturing conditions. Furthermore, it can be assumed that diffusion processes, as they occur during carbide formation during PWHT, are induced both thermally and mechanically, which should require a complete representation of the real manufacturing process in the laboratory. However, previous investigations have concentrated primarily on the influence and interaction of thermal and metallurgical factors and have neglected the mechanical influence of structural shrinkage restraint, which is present above all in thick-walled pipe constructions. Due to new, micro-alloyed material concepts with a very high degree of purity, previously known SRC causes, such as the embrittlement of the PAGB by phosphorus or sulfur segregation, are no longer the dominant factor. The influence of temperature control during welding on the resulting component stress as well as crack formation during stress-relief heat treatment under consideration of realistic manufacturing conditions, in particular the structural shrinkage restraint, has not yet been investigated.

Several studies on welding of structural steel welds under severe restraint conditions revealed significant effects and interactions regarding heat control, welding process, and the restraint of the weld [22, 23]. It was mainly observed that the occurring reaction forces and bending moments as well as the resulting stress distribution in the welded components increase as the restraint of the lateral and angular shrinkage intensifies. Particularly under high restraints typically found in the welded structures of for example petrochemical reactors, high bending stresses as a result of a build-up of unequal shrinkage forces over the welding seam height may lead to critical local mechanical loads in the weld seam and in the HAZ during welding and after cooling of the weld [24]. For high-strength structural steels, these studies have shown an understanding of how the critical transient loads during multilayer welding and the resulting residual stresses can be taken

**Table 1** Chemical composition of 13CrMoV9-10 (spark emission spectrometric analysis) in wt.%

C	Si	Mn	Cr	Cu	Mo	Ni	Ti	V	Nb	Fe
0.12	0.08	0.51	2.29	0.11	0.98	0.12	<0.01	0.30	0.03	Balance

into account by adequately adapting heat control, welding process, and welding consumables applied [24–26]. Therefore, it is necessary to transfer these findings to the SRC behavior of modern V-modified Cr-Mo-steels in order to obtain a profound understanding of the interaction with the mechanical influences during welding of real components. Part I of this study is thus concerned with the forces and stresses that occur during welding, cooling, and subsequent heat treatment.

## 2 Experimental procedure

The welding tests performed in this study were carried out on the low-alloy, carbide-forming, creep-resistant pressure vessel steel 13CrMoV9-10 (material number, 1.7703) using a welding filler of the same type<sup>1</sup>. Tables 1 and 2 show the chemical composition and its mechanical properties.

The submerged arc tandem welding process with solid wire electrodes in multilayer welding was used for the tests. All tests were carried out using the “Union S 1 CrMo 2 V”-wire electrode in combination with the “UV 430 TTR-W1”-welding flux. The wire electrode has a diameter of 4 mm. The agglomerated fluoride-based welding flux was re-dried at 350 °C for 10 h before welding. The main components of the flux, the chemical composition of the wire electrode, and the weld metal as well as the mechanical properties of the pure weld metal are listed in Tables 3, 4, and 5. The mechanical properties of the weld metal are not affected by heat treatment times longer than 8 h.

An industrial submerged arc welding (SAW) machine with tandem welding head was used. The test welds were produced by varying the heat control, in particular the preheat/interpass temperature and the heat input per unit length. The effective thermal power of the heat source was kept constant, and the adjustment of the heat input per unit length was carried out by varying the welding speed. This made it possible to adjust the deposition rate and thus the weld bead volume with almost constant arc characteristics and unaffected burn-off loss of the alloying elements. For the welding tests, the design of experiments (DoE) is used in the form of a central composite design as shown in Fig. 1. The use of DoE makes it possible to minimize the scope of the experiments through the structured setup, the targeted combination of factors, and the statistical

<sup>1</sup> ISO 24598-A—S Z CrMoV2, ISO 24598-B—SU 2C1MV

**Table 2** Mechanical properties of 13CrMoV9-10 (hardened + tempered)

Temperature in °C	Rolling direction	Yield strength	Tensile strength	Elongation at fracture	Reduction of area
		$R_{p0.2}$ in MPa	$R_m$ in MPa	$A_5$ in %	$Z$ in %
RT	Longitudinal	609	714	24	80
450		491	574	20	79
RT	Transverse	621	726	22	77
450		494	576	19	77

evaluation, and at the same time to determine as precisely as possible the cause-effect relationships between the influencing factors and the target variables.

The preheat and interpass temperature was varied in the range of  $220 \pm 40$  °C in accordance with the limit values in API Technical Report 934-B [27] and the processing recommendations of the filler metal manufacturer. The heat input per unit length was varied in a parameter window of  $35 \pm 15$  kJ/cm. This results in a non-orthogonal test plan with two independent parameters and two measurements (one repetition) at the central point (see Fig. 1). To avoid systematic errors, the experimental plan was randomized. In this way, external influences that cannot be controlled are statistically distributed and are not registered as actual influencing factors. Note that statistical analysis of the reaction stresses was limited to the inner parameter window (points a, c, e, g, and i in Fig. 1). This is because an adapted heat input was used for the outer parameter window in the root area of the joint. A summary of the welding parameters can be found in Table 6.

The welding tests were performed in a special test facility [28, 29] with a maximum load spectrum of 2 MN (tension or compression) (Fig. 1). The component load, i.e., the reaction forces and bending moments, is impressed or recorded during welding by six independently operating hydraulic cylinders. Thus, for example, the influence of process parameters on the resulting component load or the effect of stress-relieving treatments can be observed and evaluated online. Manufacturing conditions or processes can thus be transferred to the laboratory scale. The operating modes “displacement control” and “load control” are available for component simulation. If the system is in “displacement control,” the free expansion of the clamped specimen is restrained, and the heat input of the welding process results in reaction forces and bending moments in the overall system. If the system is in “load control,” the change in length of the specimen is

adjusted while maintaining the forces and bending moments applied. Both types of control were used in the investigations carried out here. The reaction forces are registered via the elastic expansion of the piston rods by means of strain gauges. The reaction moment around the longitudinal axis of the weld ( $M_x$ ) is calculated using the lever arms specified by the design [28]. The bending moment  $M_x$  results from non-uniform transverse shrinkage forces in plate thickness direction.

Two plates each with the dimensions 980 mm ( $l$ )  $\times$  250 mm ( $w$ )  $\times$  20 mm ( $h$ ) were joined. The free clamping length, i.e., the distance between the clamping jaws, was  $l_{\text{free}} = 672$  mm. The specimen halves were fixed centrally in the 2-MN test system by means of a hydraulic clamping system. Preparation of the flank angle of  $2^\circ$  was carried out by flame cutting and final grinding. The gap between the flanks was 32 mm and prepared due to tack welding of a backing and run-on/off tabs after clamping of the specimens. The restraint intensity of the weld setup (stiffness of the weld surrounding related to the length of the welded joint) was determined to be  $R_{Fy} = 2.74$  kN/(mm·mm) [30]. In this context, it was also possible to analytically determine the degree of bending restraint of the test setup and it is approximately  $R_{Mx} = 6.4$  kNm/(°/mm) [23].

The temperature profile during welding was recorded continuously, transverse to the weld seam, in the center of the specimen using four thermocouples. The distance of the thermocouples to the weld metal was 15 mm, 40 mm, 60 mm, and 100 mm.

Temperature control during preheating, dehydrogenation heat treatment (DHT; 350 °C for 2 h), and stress-relieving (PWHT, 705 °C for 8 h) was carried out by an additional thermocouple on the bottom side of the specimen (specimen center, 15 mm adjacent to the weld flank). These heat treatments were implemented using encased heating mats on the top and bottom of the specimens. The temperature control for the tests is exemplarily shown in Fig. 2 including details of the DHT and the PWHT. As can be seen, the temperatures are very close to the target values. Apart from slight overshoots in the beginning of each holding cycle, the derivation is just about 1–2 K. Welding, DHT, and subsequent PWHT took about 2 days for each test. The individual test steps are implemented as given in Table 7.

**Table 3** Main components of the welding flux (UV 430 TTR-W) in wt.%

SiO <sub>2</sub> +TiO <sub>2</sub>	CaO+MgO	Al <sub>2</sub> O <sub>3</sub> +MnO	CaF <sub>2</sub>
16	40	13	26

**Table 4** Chemical composition of the filler wire in wt.%

	C	Si	Mn	Cr	Cu	Mo	Ni	Ti	V	Nb	Fe
Union S1 CrMo 2 V <sup>1</sup>	0.09	0.04	1.24	2.39	0.01	1.01	0.02	0.001	0.26	0.015	Balance

<sup>1</sup> ISO 24598-A—S Z CrMoV2, ISO 24598-B—SU 2C1MV

During preheating, welding, and DHT, the system was operated in “displacement control” to simulate the joining of two ring segments of a pressure vessel by the restrained expansion and shrinkage [1]. In real component welds, the ring segments impede the expansion of the locally heated weld area. After the DHT, the specimen cools down to ambient temperature with shrinkage restraint.

The stress-relief heat treatment usually takes place after completion of the vessel. The entire pressure vessel is then heat-treated in a large furnace (thicknesses up to 475 mm, diameter up to 8 m, length up to 30 m, and a weight of several 100 t). Due to the almost homogeneous and slow heating, the vessel can expand freely, whereby the global reaction stresses resulting from the welding process remain until the necessary hot yield strength is reached. Nevertheless, local residual stress peaks reaching the hot yield strength during heating can relax. To simulate the actual behavior during fabrication, the 2-MN test system was operated in “load control” during the heating and cooling phases of the PWHT. This compensated for the temperature-induced expansion of the weld area and maintained the load level resulting from the welding process up to the prescribed annealing temperature of 705 °C. After reaching the target temperature, the test system switched to “displacement control,” which enabled the global relaxation of the welded joint. To characterize the influence of the heat control on the microstructure, metallographic examinations were carried out using light microscopy. The microscopy samples were taken from similar positions within the individual welded specimens. Nital was used as etchant. Occurring SRC was detected by magnetic particle inspection following ISO 17638 after cutting off the run-on/off tabs. As the weld surface structure led to several misinterpretations, the weld reinforcement was milled off to allow for crack evaluation.

### 3 Results and discussion

#### 3.1 Influence of heat control on the weld build-up and microstructure

Figure 3 shows the macro-sections of the weld seams as a function of the heat input per unit length and the preheat/interpass temperature. The subfigures are arranged following the DoE test matrix in Fig. 1 using the same labeling (a)–(i). The interpass boundaries are marked by black lines in the macro-sections. The build-up of the weld seam, the microstructure, and the characteristics of the HAZ are predominantly determined by the level of the heat input per unit length. When welding with low heat input per unit length, the weld seam consists of many narrow beads, characterized by numerous reheated zones and a small proportion of non-recrystallized microstructure (Fig. 3a, d, g). When the heat input per unit length increases, the individual weld beads become larger what leads to a growing proportion of uninfluenced, coarse microstructure in the filler layers. On the other hand, with the highest heat input per unit length of 50 kJ/cm, almost the entire previously welded beads are being tempered. Due to this, the proportion of the non-recrystallized microstructure decreases, so that the weld seam has a large proportion of fine-grained microstructure. Nevertheless, the fine-grained microstructure is limited to the lower half of the weld metal. The capping runs are characterized by coarse columnar grains which reach into the center of the weld metal due to the high penetration caused by the high heat input (Fig. 3f). The HAZ of the base material is characterized by a narrow band which widens as the heat input per unit length increases. Details about the microstructure of the HAZ are presented in part II of this work [21].

**Table 5** Mechanical properties for the weld metal, wire/flux combination: Union S 1 CrMo 2 V<sup>1</sup> + UV 430 TTR-W (manufacturer’s specification for single-wire welding on alternating current)

Heat treatment	Temperature in °C	Yield strength $R_{p0.2}$ in MPa	Tensile strength $R_m$ in MPa	Elongation at fracture $A_5$ in %	Impact absorbed energy KV in J	
					– 20 °C	– 30 °C
705 °C/10 h	RT	415	600	18	100	54
	482	365	450	16	–	–
705 °C/30 h	RT	415	600	20	100	54
	482	365	450	16	–	–

<sup>1</sup> ISO 24598-A—S Z CrMoV2, ISO 24598-B—SU 2C1MV

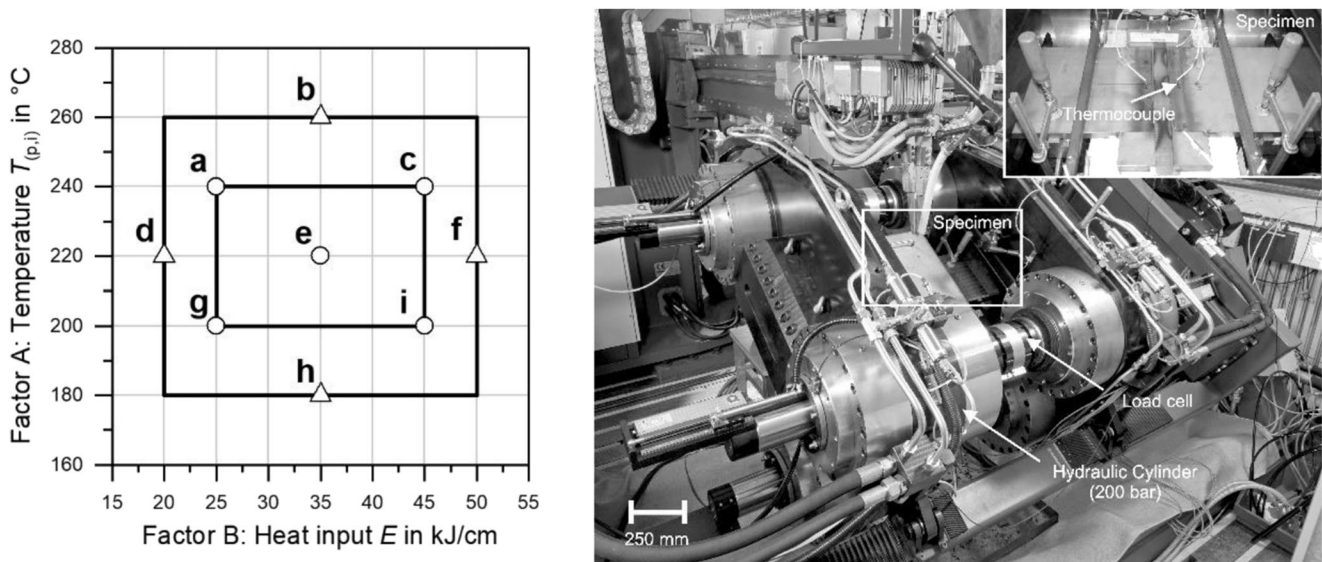


Fig. 1 Schematic representation of the central composite experimental design (left); 2-MN test facility with specimen detail (right)

### 3.2 Reaction forces and bending moments during welding

Figure 4 shows, exemplarily, the reaction force and the temperature of four individual tests during the simulated manufacturing process in the 2-MN test facility. The PWHT is not shown here as the intention is to illustrate the load occurring prior to the stress-relief treatment. The force curves show alternating tensile and compressive forces due to the cyclic heat input of welding as it is typical for high-strength steel welds [31]. While the heat input during deposition of the individual runs induced compressive forces due to local expansion of the material, each cooling to interpass temperature led to tensile forces which became highest after the completion of the last run. The local heating during subsequent DHT induced compressive forces which turned into tension after final cooling. Despite similar characteristics of the different tests, a specific reaction force for each parameter combination

is present after cooling to ambient temperature. A detailed explanation of the phenomena during preheating (I), welding (II), and DHT (III) can be found in [29]. The results of the individual tests are summarized below using a contour diagram based on the regression analysis.

The effect of the preheat/interpass temperature ( $T_{(p,i)}$  in °C) and the heat input per unit length ( $E$  in kJ/cm) on the reaction force can be assessed and quantified by means of statistical evaluation. From the reaction force, the resulting transverse stress  $\sigma_y$  (in MPa) is obtained by relating the reaction force  $F_y$  (in N) to the plate cross-section  $A$  (in mm<sup>2</sup>) (Eq. 1).

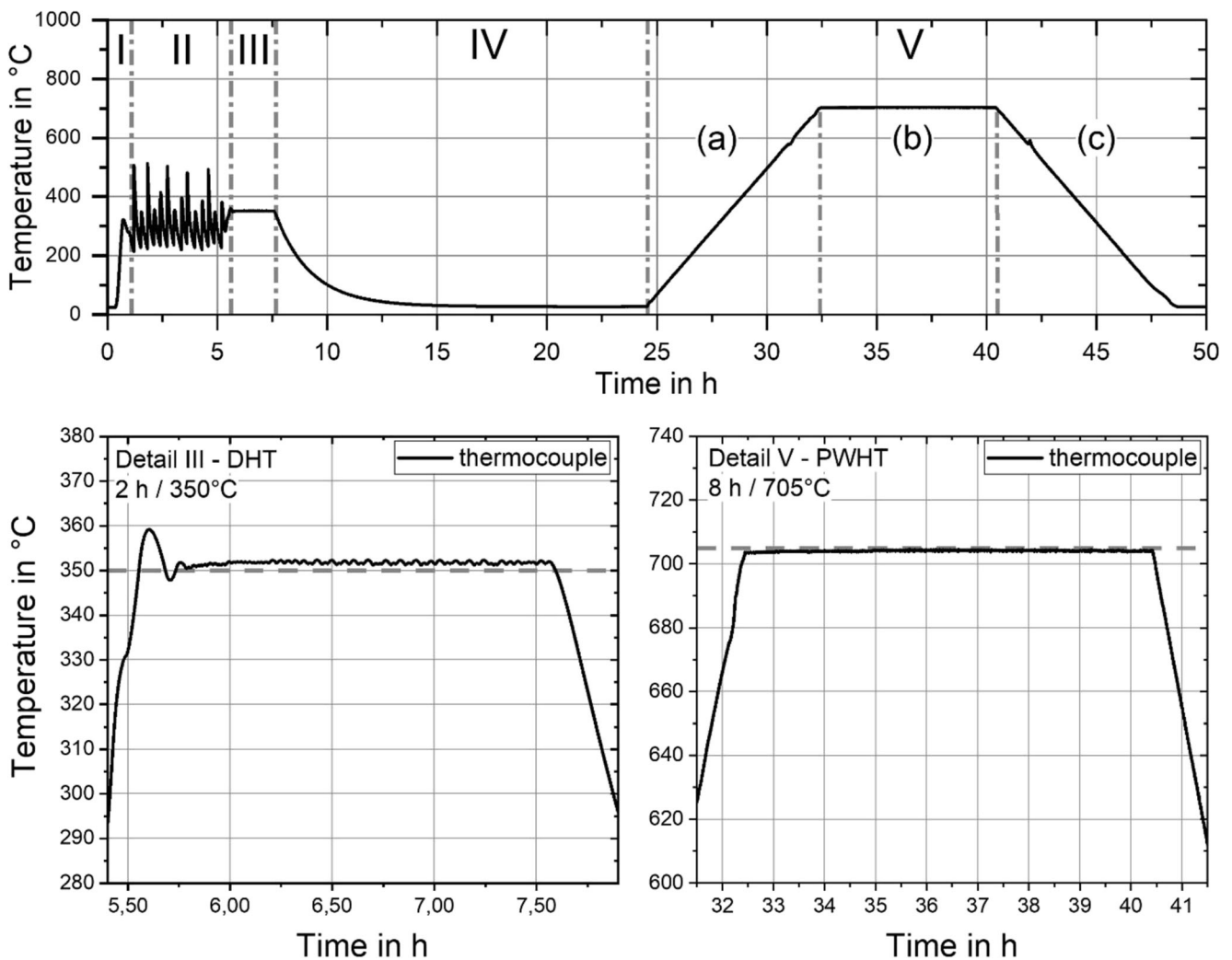
$$\sigma_y = \frac{F_y}{A} \quad (1)$$

Figure 5 (left) shows the resulting contour diagram. The greatest effect on the transverse stress is due to the interpass temperature, which is due to the temperature field expansion and the temperature level increase. The effect of the heat input per unit length is due to the disproportionately changing heat transfer into the base material by the melting filler wire but has a significantly lower effect on the transverse stresses.

In multilayer welding, the heterogeneous shrinkage of the weld metal also leads to eccentric forces which would cause distortion in non-restrained shrinking specimens. In this study, the restraint results in bending moments around the weld longitudinal axis instead. The bending moment shown in Fig. 6 is caused by the asymmetrical weld metal deposition and the resulting temperature field. Similar to the reaction force, the cyclic heat input leads to characteristic curves depending on the welding parameters. Specific bending moments were present after DHT and cooling to ambient temperature. For a detailed explanation of the formation of the bending moment

Table 6 Parameters for SAW tandem process

	Wire 1	Wire 2
Type of current	DC	AC
Wire diameter	4 mm	4 mm
Voltage	30 V	32 V
Current	600 A	550 A
Heat input	18 kW	17.6 kW
Torch angle	6° backhand	6° forehand
Torch distance	18 mm	
Welding speed	0.42–0.85 m/min	
Heat input per unit length	20–50 kJ/cm	
Preheat/interpass temperature	180–260 °C	



**Fig. 2** Temperature control during the simulated manufacturing process in the 2-MN test facility: I tacking + preheating, II welding, III DHT, IV cooling to ambient temperature, and V PWHT (heating (a), holding (b),

cooling (c)). Details of the DHT and PWHT (lower subfigures). Data exemplarily for center point test, preheating/interpass temperature 220 °C and heat input per unit length 35 kJ/cm (cf. Fig. 1)

during preheating (I), welding (II), and DHT (III), reference is made to [29].

From the bending moment  $M_x$  (in Nm), the resulting bending stress  $\sigma_{B,Mx}$  (in MPa) can be calculated by taking into account the section modulus  $W_B$  (in  $m^3$ ) of the plate cross-

section (Eq. 2). The resulting bending stress after welding and cooling to ambient temperature is mainly influenced by the heat input per unit length. The preheat and interpass temperatures, on the other hand, have almost no effect and no significant influence on the bending stresses, as the contour diagram

**Table 7** Simulated manufacturing steps according to Fig. 2

Step		Operation mode
I Tacking + preheating	Tack welding and subsequent heating to the individual preheating temperature	Displacement control
II Welding	Welding following the individual interpass temperature	Displacement control
III DHT	350 °C for 2 h	Displacement control
IV Cooling	Cooling to ambient temperature	Displacement control
V PWHT		
(a)	Heating to 705 °C by 60 K/h	Load control
(b)	Holding at 705 °C for 8 h	Displacement control
(c)	Cooling to ambient temperature by 60 K/h	Load control

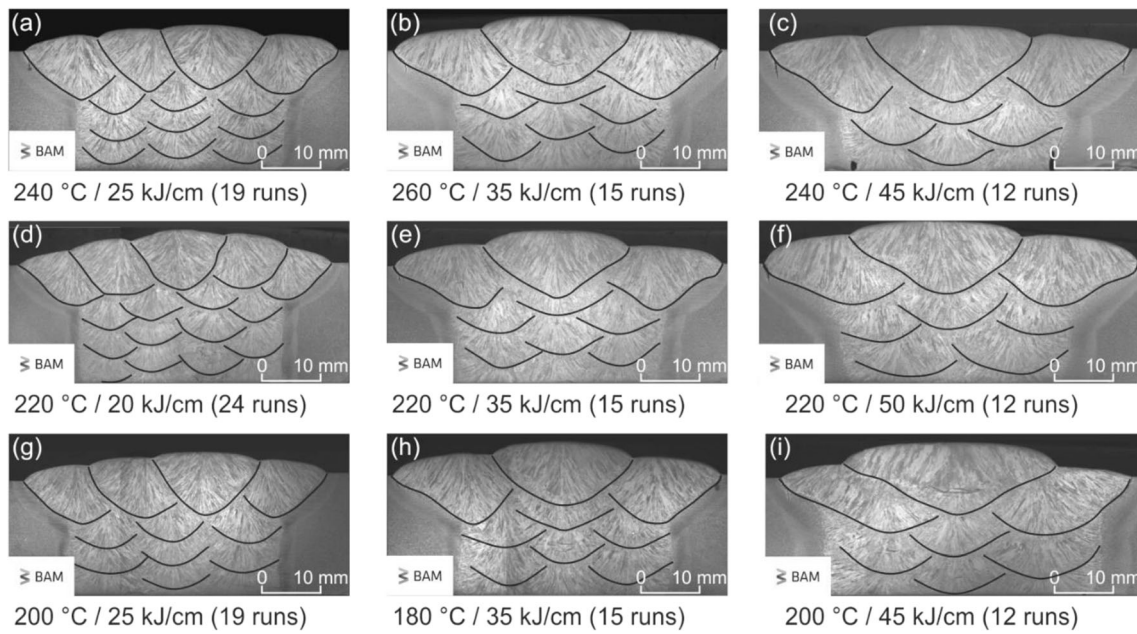


Fig. 3 Overview of the macro-sections of the welded joints as a function of the heat control (etchant: Nital)

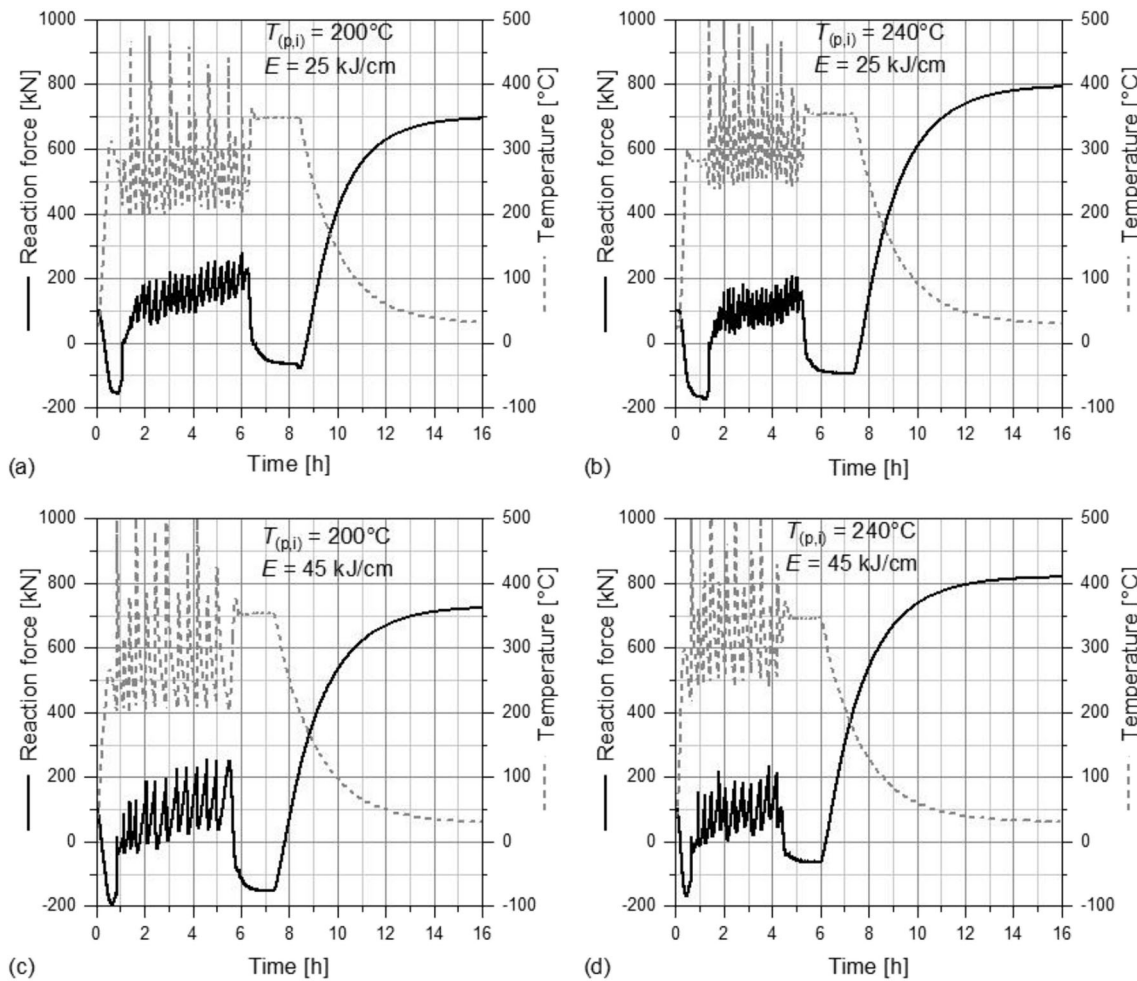
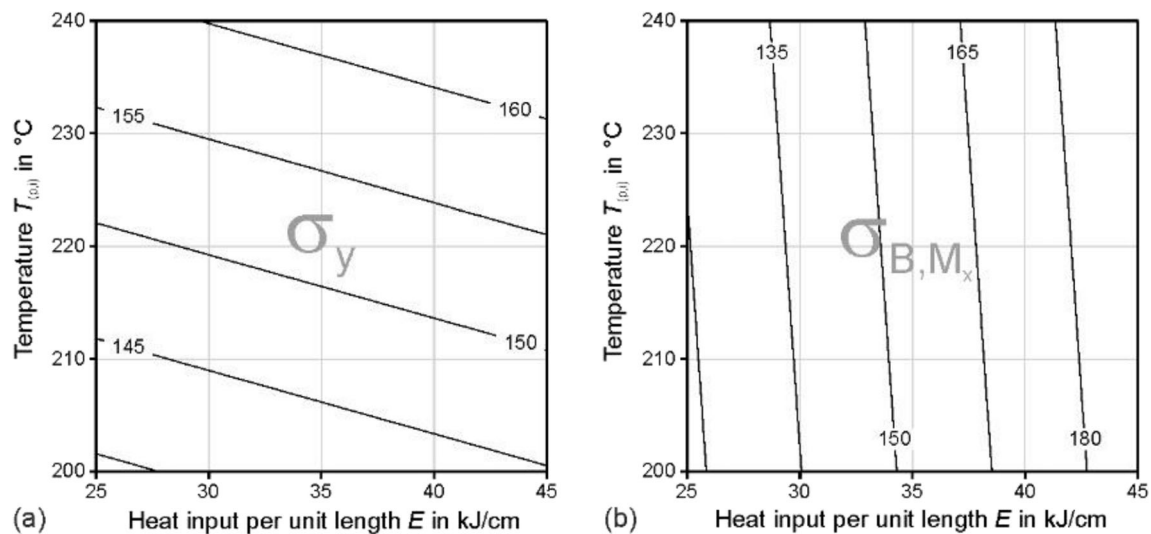


Fig. 4 Reaction force and temperature during preheating, welding, and DHT (tests a, c, g, and i cf. Fig. 1). PWHT not included



**Fig. 5** Effect of the heat input per unit length  $E$  and the preheat/interpass temperature  $T_{(p,i)}$  on the reaction stress  $\sigma_y$  [MPa] after welding and DHT prior to PWHT, linear regression,  $R^2 = 99.94\%$  (left), and effect of the heat input per unit length and the preheat/intermediate layer temperature

on the bending stress  $\sigma_{B,M_x}$ , after welding and DHT prior to PWHT, linear regression,  $R^2 = 99.96\%$  (right). Based on the inner parameter window (cf. Fig. 1, points a, c, e, g, and i)

in Fig. 5 (right) shows by means of the almost vertical contour lines.

$$\sigma_{B,M_x} = \frac{M_x}{W_B} \quad (2)$$

The heat input per unit length ( $E$  in kJ/cm) and the preheat/interpass temperature ( $T_{(p,i)}$  in °C) show a differing effect on the transverse stresses and the bending stresses. Provided a homogeneous temperature distribution in the thickness direction, the preheat/interpass temperature has a particular effect on the transverse stress, while the heat input per unit length has mainly an effect on the bending stress. The reason is that an increase in the preheat/interpass temperature solely affects the temperature level in the entire specimen cross-section but not the temperature distribution (no gradient), so that the bending stress remains virtually unaffected. On the other hand, the highly localized heat input per unit length results in localized heating of the specimen and leads to asymmetrical expansion or shrinkage, which primarily affects the bending stress. However, an increase in both parameters results in an increase in the resulting load on the welded structure.

The total reaction stress is simply calculated as the sum of the transverse stresses and the bending stresses resulting from the reaction forces and bending moments due to welding. The calculated contour diagram is shown in Fig. 7. The measured values are also included. The total reaction stress varies within the inner parameter window (cf. Fig. 1) by approx. 35% over the heat input per unit length and by 7% over the preheat/interpass temperature.

The final PWHT serves to relax the welding induced stresses to the level of the hot yield strength at 705 °C of about

190 MPa. Despite the load is maintained during heating (“load control,” cf. Table 7), local stress peaks are nevertheless relieved before the holding temperature is reached. However, stress relief cracks in the heat-affected zone occurred in all experiments as a result of the PWHT under restraint.

### 3.3 Influence of heat control on the formation of stress relief cracks

The cracks that occurred during the PWHT were detected with the help of magnetic particle crack detection. Note that no other types of cracks were found on the surface. The influence of heat control on the formation of stress relief cracks is evaluated based on the cumulative crack length. This is the sum of the length of all visually detected cracks opened to the surface. The results are given in Fig. 7 (right) ordered by the reaction stress found for every test. Two tests (c and f) with the highest loads resulted in the highest cumulative crack lengths. In both cases, the heat input and at the same time the preheat/interpass temperatures were high. Also, test b with the highest preheat/interpass temperature of 260 °C resulted in increased cracking even though the reaction stress is in the lower range. Other parameter sets showing lower heat input or lower interpass temperature or both were accompanied by less cracking. It becomes clear that the parameter combinations located in the upper right corner of the DoE (cf. Fig. 1 b, c, f) are most prone to SRC within this study. High heat input per unit length and/or high preheating/interpass temperature resulted in an increase in the cumulative crack length. At the same time, those



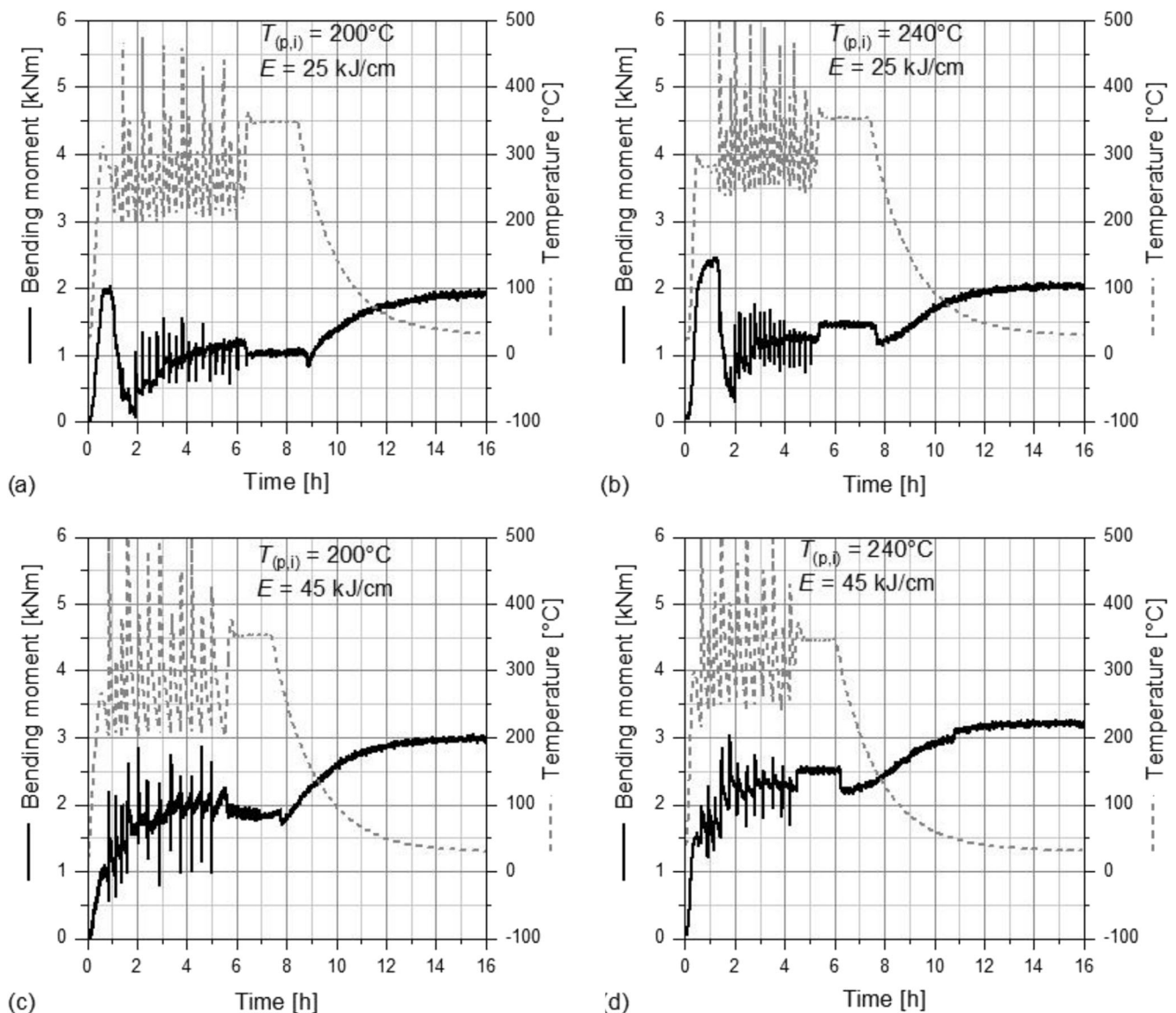


**Fig. 6** Reaction moment and temperature during preheating, welding, and DHT (tests a, c, g, and i cf. Fig. 1). PWHT not included

parameters led in tendency to an increase of the reaction stress when welding under restraint. Besides the load, mainly the microstructure and the associated mechanical properties are responsible for SRC. Their influence is discussed in part II of this study [21].

## 4 Conclusions

1. Under defined restraint, the heat control has a significant effect on the reaction forces and bending moments occurring during and after welding. High preheat/interpass temperatures lead to a significant increase of the respective transverse stresses after subsequent cooling to ambient temperature. On the other hand, an increase in the heat input per unit length is rather affecting the bending stresses.
2. Higher heat input per unit length leads to an increase of the bending stresses.
3. The total reaction stress, as the sum of the transverse and bending stresses, can thus be influenced by the heat control. In the parameter field studied, the influence of the heat input per unit length dominates over the preheat/interpass temperature, which is due to the large proportion of bending stresses in the total reaction stress.
4. Stress relief cracks in the heat-affected zone occurred in all experiments as a result of the PWHT under restraint.
5. The heat control during welding influences the SRC formation during the PWHT. The cumulative crack length, as a measure of the sensitivity to SRC, was most pronounced with high heat input and high preheating/interpass temperatures.

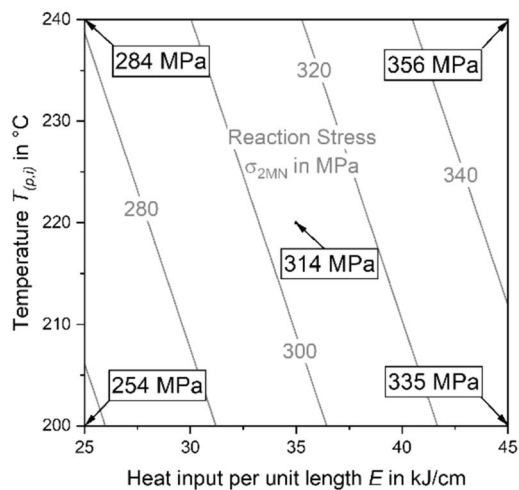
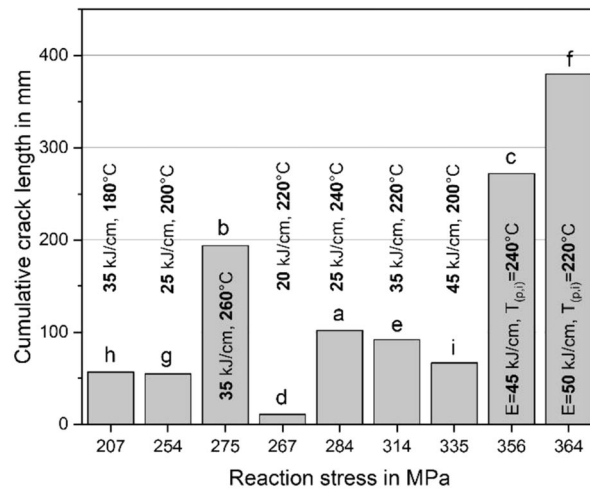


**Fig. 7** Effect of the heat input per unit length  $E$  and the preheat/interpass temperature  $T_{(p,i)}$  on the total reaction stress  $\sigma_{2MN}$  prior to PWHT, linear regression,  $R^2 = 99.69\%$ . The actual measured reaction stress is indicated



for the inner window (cf. Fig. 1 a, c, e, g, i) of the DoE (left). Cumulative crack length dependent on the reaction stress (right), parameter set indicated by a–h according to Fig. 1

**Funding** Open Access funding enabled and organized by Projekt DEAL.

**Open Access** This article is licensed under a Creative Commons Attribution 4.0 International License, which permits use, sharing, adaptation, distribution and reproduction in any medium or format, as long as you give appropriate credit to the original author(s) and the source, provide a link to the Creative Commons licence, and indicate if changes were made. The images or other third party material in this article are included in the article's Creative Commons licence, unless indicated otherwise in a credit line to the material. If material is not included in the article's Creative Commons licence and your intended use is not permitted by statutory regulation or exceeds the permitted use, you will need to obtain permission directly from the copyright holder. To view a copy of this licence, visit <http://creativecommons.org/licenses/by/4.0/>.

## References

- Antalfy L (2009) Metallurgical, design & fabrication aspects of modern hydroprocessing reactors. *Weld Res Counc Bull* 524:77–115
- Chovet C, Schmitt J (2011) Additional recommendations for welding Cr-Mo-V steels for petrochemical applications. *Weld World* 55(11–12):31–38. <https://doi.org/10.1007/BF03321540>
- Dhooge A, Vinckier A (1986) Reheat cracking – a review of recent studies. *Weld World* 24(5/6):104–126
- Lundin C, Khan KK (1996) Fundamental studies of the metallurgical causes and migration of reheat cracking in 1.25Cr-0.5Mo and 2.25Cr-1Mo steels. *Weld Res Counc Bull* 409
- Schroepfer D, Kromm A, Hannemann A, Kannengiesser T (2018) In-situ determination of critical welding stresses during assembly of thick-walled components made of high-strength steel. *Mater Res Proc* 6:191–196. <https://doi.org/10.21741/9781945291890-30>
- Bentley KP (1964) Precipitation during stress relief of welds in Cr-Mo-V steels. *Br Weld J*:507–515
- Boniszewski T ((1971)) Metallurgical aspects of reheat cracking of weldments in ferritic steels. In: Heat-treatment aspects of metal-joining processes, Proceedings of the Biennial Conference organized by the Heat Treatment Joint Committee of the Iron and Steel Institute, the Institute of Metals and Institution of Metallurgist (London: 8–9 December), p 29–41
- Chauvy C, Pillot S. : Prevention of weld metal reheat cracking during Cr-Mo-V heavy reactors fabrication. In 2009 ASME Pressure Vessels and Piping Division Conference. ASME. Prague, Czech Republic, July 2009, p 1–9
- Chauvy C (2009) Reheat cracking of weld metal A542D. In: A program to upgrade materials and process standards for fabrication of heavy wall vessels of 2.25 Cr - 1Mo - 0.25V alloy for service with hydrogen at high pressure and temperatures. Materials Properties Council Inc.
- Chauvy C, Pillot S (2009) How to prevent reheat cracking of weld metal A542D. In: API meeting. API. API, Denver
- Indacochea JE, Kim GS (1996) Reheat cracking studies on simulated heat-affected zones of CrMoV turbine rotor steels. *J Mater Eng Perform* 5:353–364
- Ito Y, Nakanishi M (1972) Study on stress relief cracking in welded low alloy steels. *Sumitomo Search* (7):27–36
- Kussmaul K, Blind D, Ewald J (1977) Investigation methods for the detection and study of stress-relief cracking. *Int J Press Vessel Pip* 5:159–180
- Meitzner CF (1975) Stress relief cracking in steel weldments. *Weld Res Counc Bull* (211):1–17
- Meitzner CF, Pense AW (1969) Stress-relief cracking in low-alloy steel weldments. *Weld J Bd.* 48:431s–440s
- Murray J (1967) Stress-relief cracking in carbon and low alloy steels. *Br Weld J*:447–456
- Nevasmaa P, Salonen J (2008) Reheat cracking susceptibility and toughness of 2% CrMoWVNb P23 steel welds. *Weld World* 52(3/4):68–78
- Younger N, Baker RG (1961) Heat-affected zone cracking in welded austenitic steels during heat treatment. *Br Weld J*:579–587
- Mullery F, Cadman R (1962) Cracking of welded joints in ferritic heat-resisting steels. *Br Weld J*:212–220
- McMahon CJ Jr, Dobbs RJ, Gentner DH Stress relief cracking in MnMoNi and MnMoNiCr pressure vessel steels. *Mater Sci Eng* 37(1979):179–186
- Kromm A, Lausch T, Schroepfer D, Rhode M, Kannengiesser T.: Influence of welding stresses on stress relief cracking during heat treatment of a creep-resistant 13CrMoV steel, part II: mechanisms of stress relief cracking during post weld heat treatment. *IIW-Doc.* II-2118-19

22. Schroepfer D, Kannengiesser T (2014) Correlating welding reaction stresses and weld process conditions for high-strength steel S960QL. *Weld World* 58:423–432
23. Schroepfer D, Kromm A, Kannengiesser T (2018) Load analyses of welded high-strength steel structures using image correlation and diffraction techniques. *Weld World* 62:459–469. <https://doi.org/10.1007/s40194-018-0566-x>
24. Schroepfer D, Kromm A, Schaupp T, Kannengiesser T (2018) Welding stress control in high-strength steel components using adapted heat control concepts. *Weld World* 63:647–661
25. Schroepfer D, Kannengiesser T (2016) Stress build-up in HSLA steel welds due to material behaviour. *J Mater Process Technol* 227:49–58
26. Dixneit J, Kromm A, Boin M, Wimpory RC, Kannengiesser T, Gibmeier J, Schroepfer D (2017) Residual stresses of LTT welds in large-scale components. *Weld World* 61:1089–1097
27. API Technical Report 934 B (2011) Fabrication considerations for vanadium-modified Cr-Mo steel heavy wall pressure vessels
28. Kromm A, Lausch T, Schroepfer D, Dixneit J, Hannemann A, Kannengiesser T (2018) From the field to the lab: real scale assessment of stresses in welded components. *Mater Perform Charact* 7(4):574–593. <https://doi.org/10.1520/MPC20170103>
29. Lausch T, Kannengiesser T, Schmitz-Niederau M (2013) Multi-axial load analysis of thick-walled component welds made of 13CrMoV9-10. *J Mater Process Technol* 213(7):1234–1240
30. Lausch T (2015) Zum Einfluss der Wärmeführung auf die Rissbildung beim Spannungsarmglühen dickwandiger Bauteile aus 13CrMoV9-10. Dissertation, BAM Bundesanstalt für Materialforschung und -prüfung, BAM Dissertationsreihe Band 134. Otto-von-Guericke-Universität Magdeburg, Berlin (in German)
31. Kannengiesser T, Lausch T, Kromm A (2011) Effects of heat control on the stress build-up during high-strength steel welding under defined restraint conditions. *Weld World* 55(7–8):58–65

**Publisher's note** Springer Nature remains neutral with regard to jurisdictional claims in published maps and institutional affiliations.